GSI

GSI-Preprint-98-12
Februar 1998

HEAVY NEUTRON-DEFICIENT RADIOACTIVE BEAMS: FISSION STUDIES AND FRAGMENT DISTRIBUTIONS

K.- H. Schmidt, C. Böckstiegel, A. Grewe, S. Steinhäuser, J. Benlliure, H.-G. Clerc,A. Heinz, M. de Jong, A. R. Junghans, J. Müller, M. Pfützner, B. Voss

(Contribution to the XXXVI International Winter Meeting on Nuclear Physics, Bormio, 1998)

Gesellschaft für Schwerionenforschung mbH
Planckstraße 1 • D-64291 Darmstadt • Germany
Postfach 11 05 52 • D-64220 Darmstadt • Germany

Contribution to the XXXVI International Winter Meeting on Nuclear Physics, Bormio, 1998

Heavy neutron-deficient radioactive beams: fission studies and fragment distributions

K.-H. Schmidt[a], C. Böckstiegel[b], A. Grewe[b], S. Steinhäuser[b], J. Benlliure[a], H.-G. Clerc[b], A. Heinz[a], M. de Jong[b], A. R. Junghans[b], J. Müller[b], M. Pfützner[c], B. Voss[a]

[a]*Gesellschaft für Schwerionenforschung m.b.H., Planckstraße 1, 64291 Darmstadt, Germany*

[b]*Technische Hochschule Darmstadt, Institut für Kernphysik, Schloßgartenstraße 9, 64289 Darmstadt, Germany*

[c]*Institute of Experimental Physics, University of Warsaw, Ul Hoza 69, 00-381 Warszawa, Poland*

Abstract. The secondary-beam facility of GSI Darmstadt was used to study the fission process of short-lived radioactive nuclei. Relativistic secondary projectiles were produced by fragmentation of a 1 A GeV ^{238}U primary beam and identified in nuclear charge and mass number. Their production cross sections were determined, and the fission competition in the statistical deexcitation was deduced for long isotopical chains. New results on the enhancement of the nuclear level density in spherical and deformed nuclei due to collective rotational and vibrational excitations were obtained. Using these reaction products as secondary beams, the dipole giant resonance was excited by electromagnetic interactions in a secondary lead target, and fission from excitation energies around 11 MeV was induced. The fission fragments were identified in nuclear charge, and their velocity vectors were determined. Elemental yields and total kinetic energies have been determined for a number of neutron-deficient actinides and preactinides which were not accessible with conventional techniques. The characteristics of multimodal fission of nuclei around ^{226}Th were systematically investigated and related to the influence of shell effects on the potential energy and on the level density between fission barrier and scission. A systematic view on the large number of elemental yields measured gave rise to a new interpretation of the enhanced production of even elements in nuclear fission and allowed for a new understanding of pair breaking in large-scale collective motion.

INTRODUCTION

During the last years secondary beams became available in many laboratories. Numerous experiments with short-lived radioactive projectile nuclei have initiated important progress in the understanding of nuclear structure, in particular for exotic nuclei far from the beta-stability line. While most of the activities concentrated on rather light nuclei -- ^{11}Li is a famous example -- the present work reports on a first series of experiments using beams of heavy, short-lived radioactive nuclei in order to extend our knowledge on nuclear fission in several aspects. The experiments have been performed at GSI Darmstadt, the only laboratory where relativistic secondary beams of fissile nuclides are available. An impression on the large number of nuclear species which are produced by the fragmentation of relativistic ^{238}U projectiles in a lead target is given by the calculated nuclide distribution shown in FIGURE 1. The calculation may be compared to measured data presented in ref.(1).

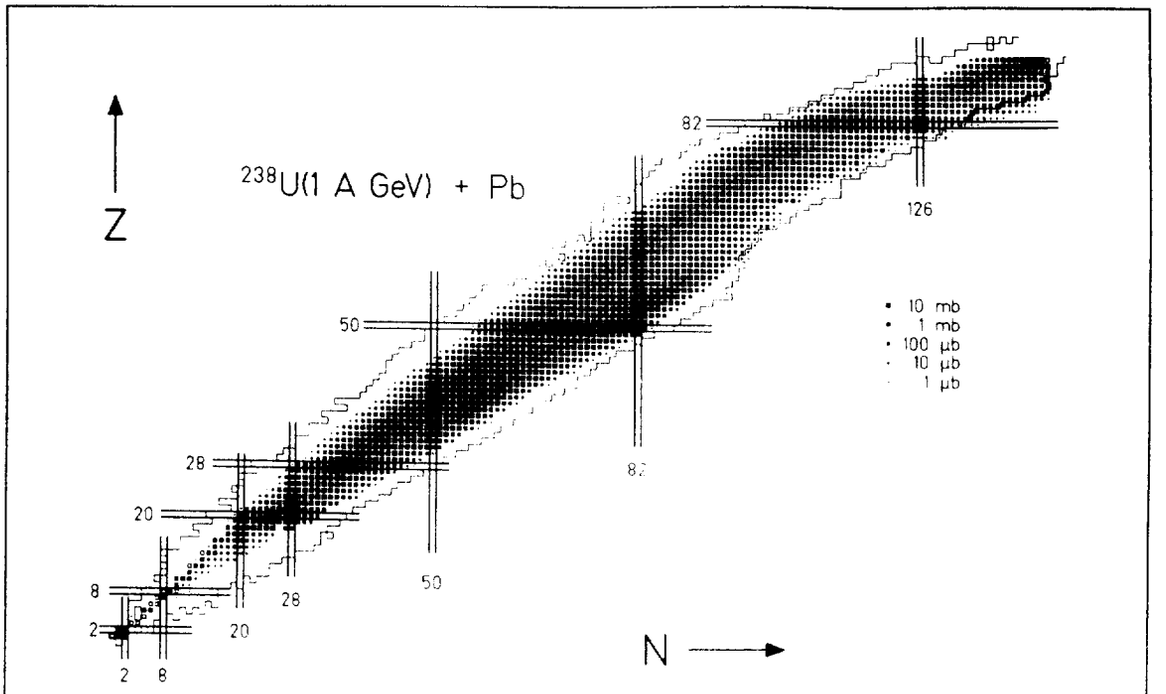

FIGURE 1: **Calculated nuclide production cross sections of the reaction ^{238}U (1 *A* GeV) + Pb. The model applied for the calculation is described in ref. (2).**

In particular, the following topics are considered in the present contribution:

1. The degree of collectivity of nuclear excitations at excitation energies which are not accessible to nuclear spectroscopy is still experimentally unexplored. The nuclear level densities which are decisive for the fission competition in the statistical deexcitation phase of excited nuclei represent an alternative access to this problem. The fragmentation of ^{238}U projectiles opens up new experimental possibilities to this field.

2. Nuclear fission provides unique information on the reordering of nucleons in large-scale collective motion. The signatures of shell structure and pairing correlations show up in fission from low excitation energies. They have general implications on the influence of shell structure on nuclear dynamics and on the viscosity of cold nuclear matter. The use of secondary beams gives access to a large new field of fissioning systems by overcoming restrictions of conventional experimental techniques.

Collective excitations

Data on fission probabilities are relevant for the understanding of structural effects in the nuclear level density. They relate the level densities of neighbouring nuclei in different configurations -- the density of transition states of the fissioning nucleus above the fission barrier and that of the daughter nucleus after neutron evaporation in its ground-state shape. By simultaneously analysing the fission probabilities of a large number of nuclei, the level density in the strongly deformed saddle-point may serve as a reference for structural and collective effects in different nuclei with spherical and deformed shapes in the ground state. In particular, one may expect new results on one of the fundamental questions of nuclear physics, namely up to which excitation energies collective nuclear excitations may persist. Several theoretical estimates have been given for the loss of col-

lectivity of nuclear excitations as a function of nuclear temperature (e. g. (3,4)), but no experimental verification has been performed up to now.

The fragmentation of ^{238}U projectiles is particularly interesting, because long isotopic chains of proton-rich nuclei crossing the 126-neutron shell are simultaneously produced. In addition, the interpretation is not complicated by large angular-momentum effects, since the fragmentation introduces low angular momenta (around 15 h) only (5). Therefore, this reaction offers unique possibilities to study the fission probabilities of highly fissile spherical shell-stabilized nuclei. In this sense they represent a test case for the predicted but not yet reached spherical superheavy nuclei around $N = 184$.

Shell structure

Separate components appear in the yields and in the kinetic-energy distributions of fission fragments due to the shell structure in the potential-energy landscape in the highly deformed fissioning system. These components are attributed to "fission channels" which are identified with valleys in the potential energy in the direction of elongation due to shell effects (6,7). There exist models which relate the properties of the fission fragments to the properties of the scission configuration (8,9). Others expect a decisive influence of the shell effects at the saddle point (10,11,12,13).

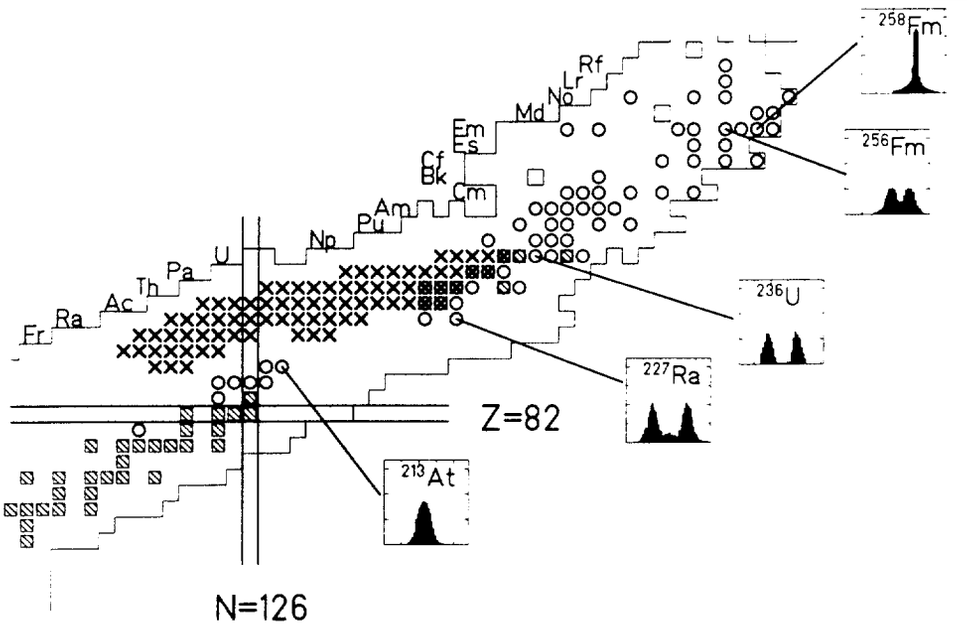

FIGURE 2: **Present knowledge on low-energy fission. Hatched squares: stable isotopes, circles: previously measured mass distributions for $E^* - B_f < 10$ MeV, crosses: this experiment. Additionally, examples of fission-fragment mass distributions are shown.**

The status of the present knowledge on low-energy fission is sketched in FIGURE 2. Studies on low-energy fission were restricted to about 80 fissioning nuclei up to now. They represent only about 10 percent of all known nuclei with Z above 82. The fission of most of them can rather well be described by a superposition of two mass-asymmetric fission channels: standard I with a spherical heavy fragment around the 82 neutron shell and standard II with a deformed heavy fragment around the 86 neutron shell. In particu-

lar at higher excitation energy, a third fission channel appears, the superlong, mass-symmetric component. Only for a very limited number of nuclei around ^{259}Fm, a very specific symmetric fission channel shows up with a narrow mass distribution and exceptionally high kinetic energies (14,15,16) which is interpreted as the formation of two spherical fission fragments near the doubly magic ^{132}Sn (17,18,19,20). Near ^{227}Ac triple-humped mass distributions have been measured (21,22,23,24,25,26,27,28,29), and around ^{213}At symmetric fission prevails (30). In the present work, we perform a systematic study of the transition from mass-symmetric fission around ^{213}At to mass-asymmetric fission above ^{233}U (see FIGURE 2). An overview on this transition is not yet available due to the lack of long-lived isotopes, necessary as target material for conventional fission experiments.

Pairing correlations

In low-energy fission, the production of fission fragments with an even number of protons and neutrons was found to be generally enhanced. This was interpreted as a measure for the probability that completely paired configurations are preserved up to the scission point. If fission starts from a completely paired superfluid configuration or from a configuration with a definite number of quasiparticle excitations, the amount of enhancement of even splits is connected to the dissipation in the fission process which couples intrinsic excitations and collective motion. Thus, it is a unique source of information on the viscosity of cold nuclear matter.

Since the complete identification of fission fragments in nuclear charge and mass number is very difficult, even-odd effects in the yields as a function of proton or neutron number only exist for a very limited number of systems. In contrast to mass yields, which are available more frequently, the elemental yields are particularly interesting, since they are not modified by the evaporation of neutrons from the excited fission fragments. In the available data, the even-odd effect in elemental yields for different fissioning systems varies as a function of fissility. In addition, for some of the systems, a variation as a function of the charge split is found. This has been interpreted as a corresponding variation of the dissipated energy (31).

With the new experimental technique applied in the present work, elemental yields can be determined with high quality for a large number of fissioning systems. Therefore, the study of pairing correlations in the fission process is another subject of interest followed here.

EXPERIMENT

The secondary-beam facility of GSI Darmstadt provides secondary beams of neutron-deficient heavy nuclei produced by fragmentation of ^{238}U. Within the intensity limits given by the primary-beam intensity and the fragmentation cross sections, nuclear charge und mass number of the secondary projectiles can freely be selected by accordingly tuning the fragment separator (32).

In a first experiment, the isotopic cross sections of elements between ytterbium and uranium produced in the fragmentation of ^{238}U at 950 A MeV in copper targets (205 and 1039 mg/cm^2) were systematically mapped (33,34). The fragment separator was operated as a momentum-loss achromat (35), using an intermediate degrader of 3.5 g/cm^2

aluminum. For the isotopical identification, scintillation detectors (36) were used to measure the positions of the fragments at the center and at the exit of the fragment separator as well as their time-of-flight. A detailed description of the identification method can be found in ref. (37).

In the secondary-beam experiment, performed later, isotopically identified secondary beams of a number of neutron-deficient preactinides and actinides were produced by fragmentation from a 1 *A* GeV ^{238}U primary beam in a 657 mg/cm^2 beryllium target. The target was coated downstream with a 212 mg/cm^2 niobium layer to increase the fraction of fully stripped fragments.

In order to study the fission properties of the secondary projectiles, excited states in the desired energy range had to be populated, and the fission products had to be detected. The specific properties of the secondary beams do not allow to use excitation mechanisms usually applied for low-energy fission studies, like the capture of thermal neutrons. Instead, dedicated experimental methods had to be developed. Since the secondary-beam intensities only reach hundred per second or less for a specific isotope, it is crucial to ensure a high secondary reaction rate and a large detection efficiency. As excitation mechanism, electromagnetic interactions with a heavy target material have been chosen. They essentially populate the giant dipole resonance with a mean energy only a few MeV above the fission barrier with cross sections as high as a few barn.

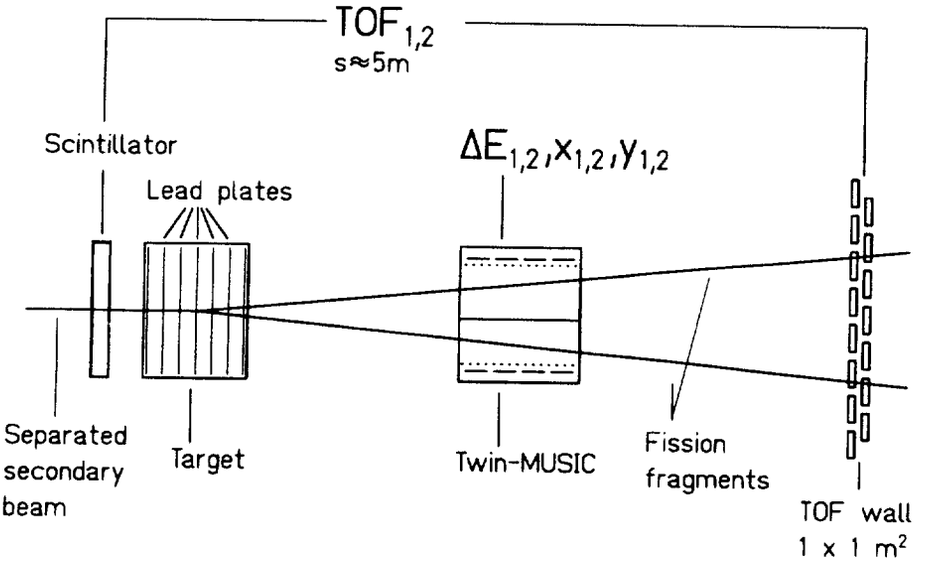

FIGURE 3: **Schematical drawing of the set up for the fission experiment mounted behind the fragment separator**

The experimental set up behind the fragment separator is sketched in FIGURE 3. As secondary target we used a stack of lead foils with a total thickness of 3 g/cm^2 mounted in a gas-filled chamber which acts as a subdivided ionization chamber (active target). With this device it is possible to determine the lead foil in which fission took place and to discriminate against fission induced in the scintillator. The average energy of the secondary projectiles in the lead target was about 420 *A* MeV. The differential energy loss of each fission fragment was measured separately with an horizontally subdivided twin ionization chamber. In order to correct the energy loss for the velocity dependence, the time-

of-flight of the fission fragments was measured by means of a (1m × 1m) scintillator wall.

FIGURE 4 shows the nuclear-charge response of the experimental set up for fission fragments after electromagnetic-induced fission of ^{226}Th. Due to the high center-of-mass energies, an excellent charge resolution is achieved. Events stemming from reactions at lower impact parameters with nuclear contact were suppressed. For details of the analysis procedure see refs. (38,39).

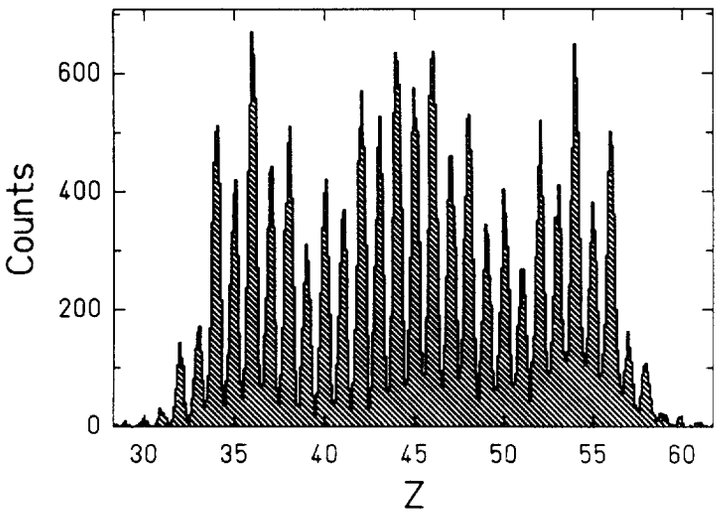

FIGURE 4: **Nuclear-charge response of the twin MUSIC with velocity correction applied as obtained for the fission fragments after electromagnetic excitation of ^{226}Th projectiles.**

RESULTS AND DISCUSSION

Influence of fission on the fragmentation cross sections

Production cross sections of long isotopic chains of elements between ytterbium and uranium were determined and compared with an abrasion-ablation model calculation (40,41). The requirement to simultaneously describe this whole body of data imposed strong restrictions on the model description. Another important constraint is given by the necessity to reproduce a series of isotopic production cross sections from ^{208}Pb fragmentation (37) where the influence of fission is almost negligible.

Part of the data together with model calculations using different options for the nuclear level densities are shown in FIGURE 5. First, it is obvious that the cross sections are very sensitive to the fission competition in the deexcitation phase: A calculation where fission is artificially suppressed overestimates the cross sections of the neutron-deficient isotopes by several orders of magnitude. But also the second option which deduces the nuclear level density from the independent-particle model, disregarding any collective excitations, deviates appreciably from the data. This calculation predicts a strong reduction of the fission competition for nuclei near the N=126 shell. Although the ground-state shell effect of these nuclei is known to reach more than 5 MeV, any stabilization of these nuclei against fission is not observed experimentally. The inclusion of the

enhancement of the level density due to collective rotations according to the theoretical expectation (4) on the other hand overestimates the fission probabilities by a large amount. Only by applying a deformation-independent damping of the rotational enhancement at about 40 MeV and an increased vibrational enhancement of the level density in spherical nuclei, the data can be reproduced. Details on the model calculations are reported in ref. (34).

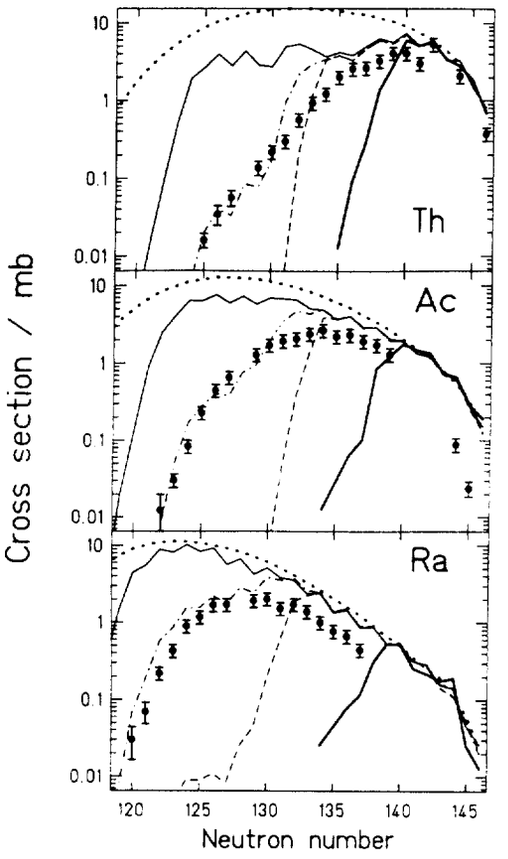

FIGURE 5: **Production cross sections of thorium, actinium, and radium fragments from a 950 *A* MeV ^{238}U beam in a copper target are shown as data points. The dotted line represents the result of a calculation without considering fission. The thin full lines result from a calculation using intrinsic level densities without including collective excitations. The thick full lines show a calculation including rotational enhancement for ground-state deformed nuclei with the damping of $K_{rot}(E)$ according to Hansen and Jensen (4). The dashed lines are calculated with rotational enhancement but with damping independent of deformation, and the dash-dotted lines include in addition vibrational enhancement for nuclei with a spherical ground state.**

Obviously, the fragmentation of ^{238}U provides new information on the collectivity of nuclear excitations beyond the applicability of spectroscopic methods. Although this information is indirect, the data clearly reveal that the nuclear level density cannot be described properly by the intrinsic level density formulated in the independent-particle model. The present analysis shows that the fission probability of excited nuclei with a spherical ground-state shape cannot be described when collective excitations are disregarded. In particular, the production cross sections for spherical superhaevy nuclei around $N = 184$ would drastically be overestimated.

Fission channels

In the secondary-beam experiment, the elemental yields and the total kinetic energies of a series of neutron-deficient preactinides and actinides from ^{205}At to ^{234}U have been determined. The elemental yields covering the transition from symmetric fission at ^{221}Ac to asymmetric fission at ^{233}U are shown in FIGURE 6. In the transitional region, around ^{226}Th, triple-humped distributions appear, demonstrating comparable weights for symmetric and asymmetric fission.

The weights of the two main fission components observed in the yields, the symmetric and the asymmetric contributions, were quantitatively determined by fitting three Gaussian curves to the charge-yield distributions: Two Gaussians represent the asymmetric component and one Gaussian is sufficient to fit the symmetric component. The width of the symmetric component was fixed to 9.5 charge units (FWHM) in all cases. This value was deduced from isotopes fissioning purely symmetrically. The ratio of symmetric to asymmetric fission was then determined by the ratio of the areas of the Gaussians describing the data.

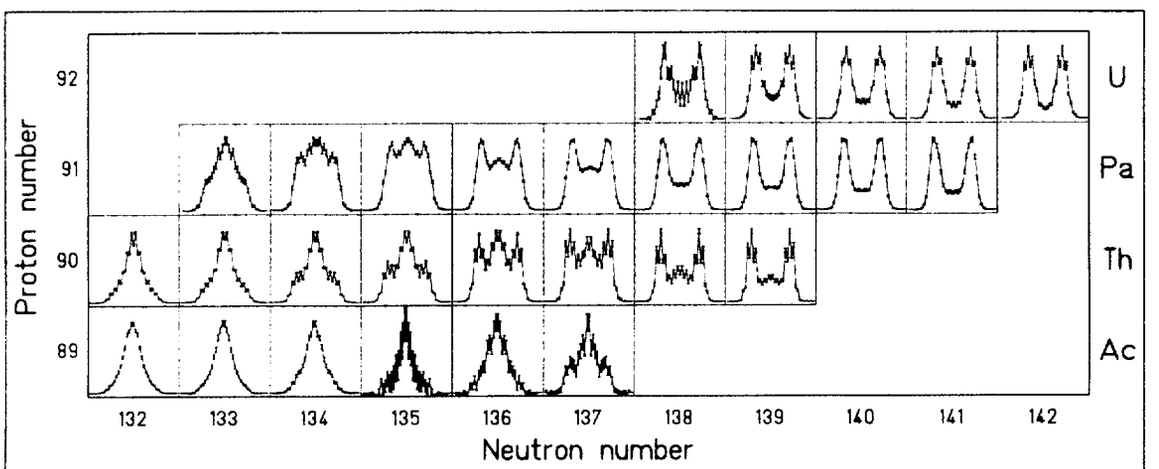

FIGURE 6: **Measured fission-fragment charge distributions from ^{234}U to ^{221}Ac are shown on a chart of the nuclides.**

The results of this procedure are shown in FIGURE 7. For all nuclei with A < 220, the symmetric component has been found to prevail. The transition is rather smooth, and the weights of the two fission components have been found to scale with the mass of the fissioning nucleus.

In detail, the charge-yield distributions and the total kinetic energies of ^{233}U, ^{228}Pa, ^{226}Th, ^{223}Th, ^{219}Ac, and ^{214}Ra are shown in FIGURE 8. For the uranium and thorium isotopes, a strong even-odd structure is observed for both the asymmetric and the symmetric component. The gross structural effects observed in the charge yields are different from those showing up in the total kinetic energies. From ^{233}U to ^{223}Th, the weight of the asymmetric fission component decreases, while the enhancement of the total kinetic energies (with respect to the expectation of the macroscopic model) for fission with a neutron number of the heavy fragment around $N = 82$ is preserved. For the lighter fissioning nuclei, another double-humped structure appears in the enhancement of the total kinetic energies while the charge distributions stay single humped. In all cases, the total kinetic

energies follow rather closely the structure of the Q values as a function of the charge split.

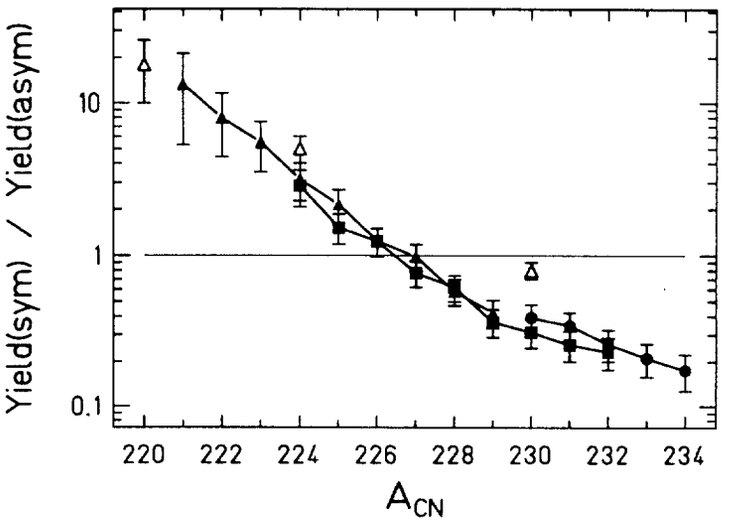

FIGURE 7: **Intensity ratios of the symmetric and the asymmetric fission components in the transitional region as a function of mass number. The full triangles (squares, circles) correspond to thorium (protactinium, uranium) isotopes. The open symbols for ^{220}Th and ^{224}Th measured by Itkis et al. (29) and for ^{230}Th measured by Unik et al. (23) are included.**

In a simultaneous description of elemental yields and total kinetic energies, these data could not be reproduced with the assumption of two fission channels, a symmetric and an asymmetric one. Since the position of the maximum in the total kinetic energies does not coincide with the maximum in the yields, it was necessary to introduce a third fission channel. According to ref. (7), each channel was represented by a Gaussian contribution in the yields and a specific scission-point configuration. Position and width of the Gaussians in nuclear charge as well as the tip distance of the scission configuration were treated as free parameters for each component. FIGURE 9 shows that a good description of both, the elemental yields and the total kinetic energies is achieved for the fissioning systems ^{223,226,2228}Th. The parameters, in particular the relative heights of the total kinetic energies, attributed to the individual fission channels, roughly coincide with the expectations for the three most intense channels known from heavier fissioning systems (see e. g. ref. (7)). In the nomenclature of Brosa et al. (7) these are standard I at $N = 82$, standard II near $N = 86$, and superlong at symmetry.

This finding also agrees with the results of Itkis et al. (29) who investigated fission of neutron-deficient actinides from appreciably higher excitation energies induced by sub-barrier heavy-ion fusion reactions.

Although the dispersion of the total kinetic energy could not be deduced in the present secondary-beam experiment due to the limited resolution in velocity and angle for single events, the relative weights of the two asymmetric fission channels could still be determined by applying a simultaneous fit to the elemental yields and the total kinetic energies. However, as an essential assumption we postulated that the compactness of the scission configuration, parametrized by the effective tip distance, does not vary inside a specific fission channel. This is in agreement with the fission model of Brosa et al.(7). The analysis showed that the triple-humped fission-fragment distributions are composed of strong contributions of three fission channels. This is true not only for the systems

shown in FIGURE 9 but also for neighbouring nuclei showing triple-humped charge-yield distributions.

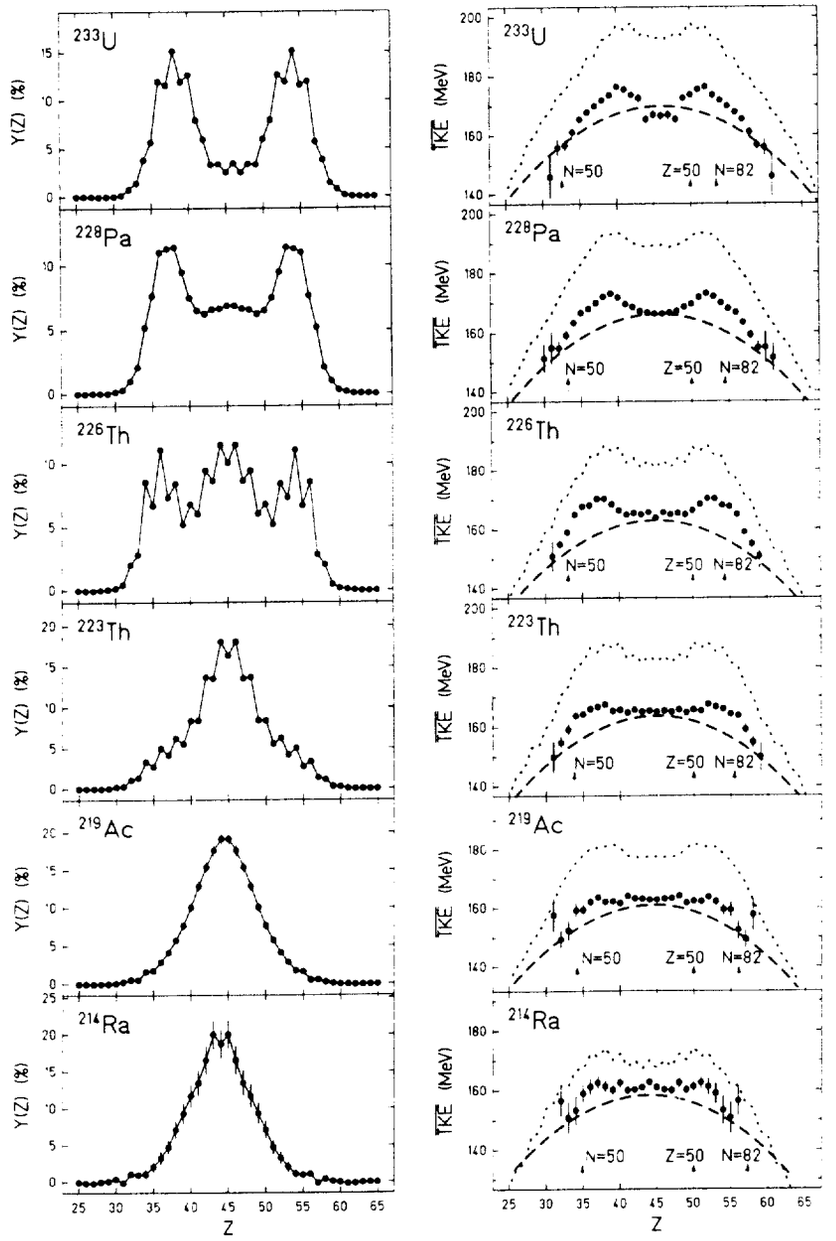

FIGURE 8: **Measured elemental yields (left part) and average total kinetic energies (right part) as a function of the nuclear charge measured for fission fragments of several fissioning nuclei. Only statistical errors are given. The total kinetic energies are subject to an additional systematic uncertainty of 2 %, common to all data (39). In addition, for each charge split the maximum Q (ground-state to ground-state) value determined by varying the neutron numbers of the fission fragments is shown. Arrows indicate the positions of neutron (N = 50, 82) and proton shells (Z = 50). The positions of the neutron shells are calculated from the proton numbers by assuming an unchanged charge density (UCD). Finally, the expectations of a macroscopic scission-point model are shown (dashed lines) based on the Coulomb repulsion of the fragments at scission including a quadrupole deformation of β = 0.625 and a tip distance of 2 fm.(3).**

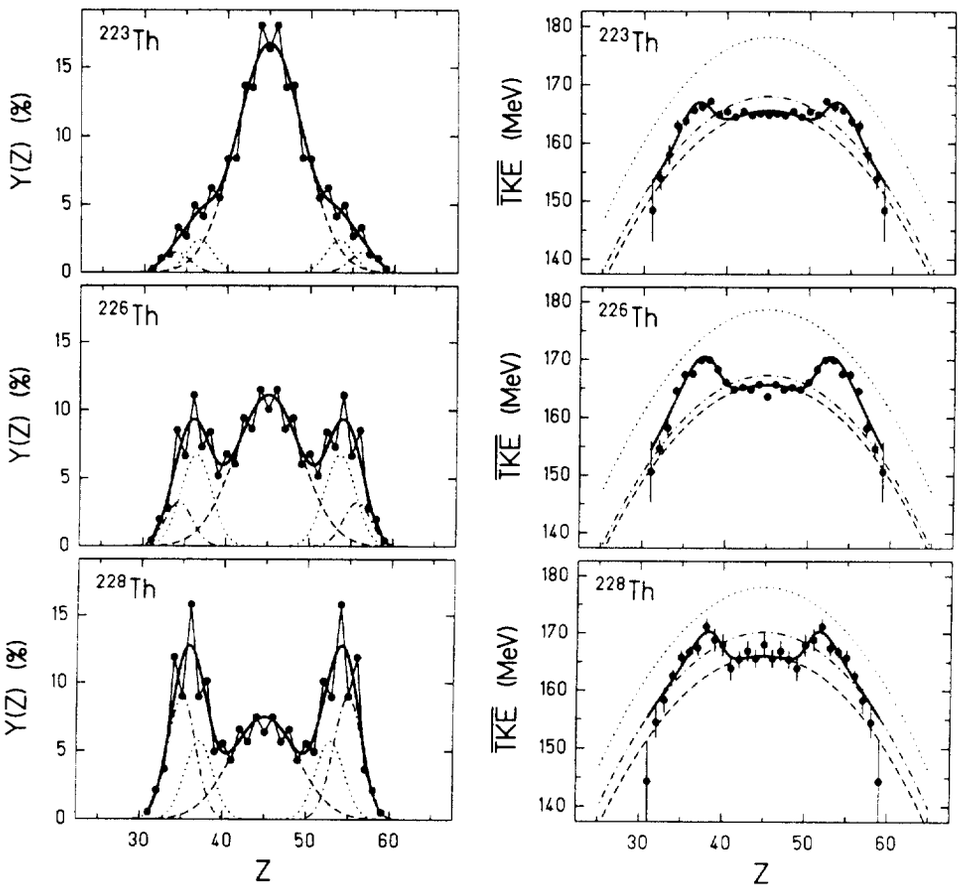

FIGURE 9: **Elemental yields and total kinetic energies for electromagnetic-induced fission of ^{223,226,228}Th. In addition to the data points, fits with three fission channels are shown as full lines. The yields and the total kinetic energies of the individual contributions are shown separately by different lines.**

The data on elemental yields support the idea, stated by Itkis et al. (42), that the weights of the fission channels are principally determined by an interplay of the neutron shells at $N = 82$ and $N = 86$ with the liquid-drop potential. A quantitative formulation of this idea has been developed by J. Benlliure et al. (43) by relating the charge distributions to the density of transition states in the vicinity of the outer fission barrier. The total kinetic energies, however, seem to be closely related to the ground-state properties of the fission fragments. This finding agrees with the expectation that the total kinetic energies are essentially determined by the shell effects in the scission-point configuration.

Pair breaking in fission

The excellent nuclear-charge resolution of the present experiment allowed to determine the even-odd structure in the elemental yields for a large number of fissioning systems. FIGURE 10 and FIGURE 11 display the experimental results for four fissioning

nuclei. In the lower part, the corresponding local even-odd effect $\delta(Z)$ of the charge distributions is shown which is defined as (44):

$$\delta(Z+3/2) = 1/8\,(-1)^{Z+1}\,\{-\ln Y(Z) + 3\ln Y(Z-1) - 3\ln Y(Z+2) + \ln Y(Z+3)\} \qquad (1)$$

Herein, $Y(Z)$ are the elemental yields. Thus, $\delta(Z+3/2)$ is a quantity measured over four consecutive yields, centered at $(Z+3/2)$. This quantity describes the local deviation from a Gaussian-like distribution.

The local even-odd effect shows a striking result for ^{220}Ac and ^{228}Pa: For these odd-Z fissioning nuclei, the values of $\delta(Z)$ tend to be positive for the light fragments and negative for the heavy fragments. Absolute values up to more than 0.2, that means by 20 % enhanced production yields of even elements, are found for the extremely asymmetric light charge splits. This behaviour of the local even-odd effect is found to be essentially the same for the two nuclei, although their charge distributions show very different characteristics.

For the even-Z fissioning nuclei ^{226}Th and ^{233}U, a completely different behaviour of the local even-odd effect is observed. As expected, the local even-odd effect is positive throughout. However, there is a strong variation from a minimum value near symmetry to an increase of about a factor of two in the extremely asymmetric charge splits. Again, this behaviour proves to be rather general, independent of the gross structure of the charge distribution. This finding goes in line with previous observations in ^{235}U(n_{th},f) (45) and ^{249}Cf(n_{th},f) (46).

The observation of even-odd effects in odd-Z fissioning nuclei and the variation of the even-odd effect as a function of the charge split in both odd-Z and even-Z fissioning nuclei can be interpreted with the assumption that unpaired protons are distributed to the nascent fragments according to the available phase space. Any intrinsic excitations induced during the descent from saddle to scission are assumed to be carried by unpaired nucleons. Thus, these nucleons populate excited single-particle states. On the way to scission, the single-particle states of the fissioning system evolve to states of the individual fragments. A quantitative formulation of this approach, based on the density of quasiparticle excitations as formulated by Strutinsky (47), is given in ref. (48). As an essential result, the local proton even-odd effect for a given number N of unpaired protons is given by the following relation:

$$\delta(Z) = (1 - 2\,Z/Z_{CN})^{N} \qquad (2)$$

where Z is the nuclear charge number of the fission fragment and Z_{CN} the nuclear charge number of the fissioning nucleus. In this expression, shell effects in the single-particle level scheme are disregarded. The data shown in FIGURE 11 can be reproduced fairly well when a fraction of 10 % for the fully paired configuration and a fraction of 90 % for one proton pair broken are assumed. In the odd-Z fissioning systems, shown in FIGURE 10, a fraction of 10 % refers to one unpaired proton and a fraction of 90 % refers to three unpaired protons.

This model at least partly explains the strongly enhanced even-odd effect observed previously in the asymmetric tails of the nuclear-charge distributions in the fission of the even-Z nuclei ^{236}U (45) and ^{250}Cf (46) without assuming particularly low intrinsic excitation energies in extremely asymmetric fission. Also the well known increase of

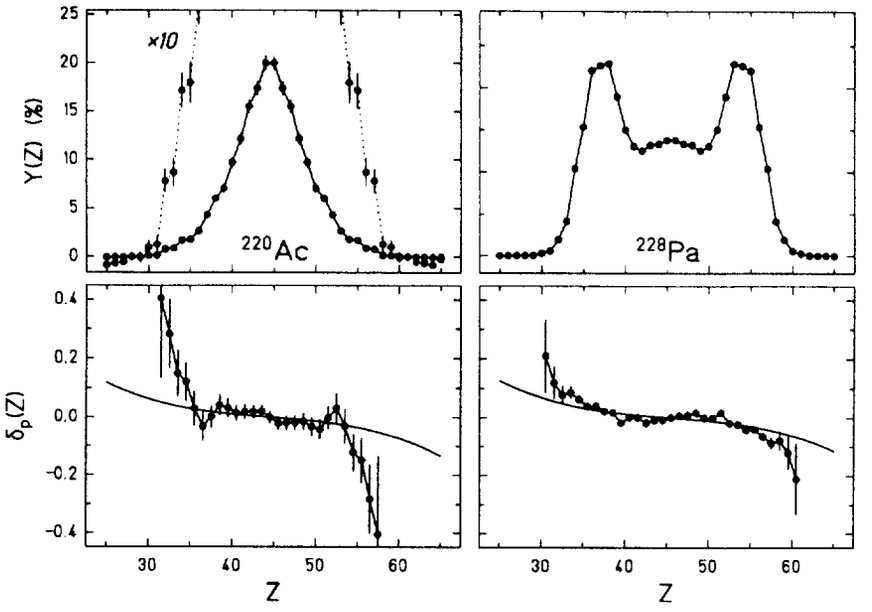

FIGURE 10: **In the upper part, the charge distributions $Y(Z)$ of ^{220}Ac and ^{228}Pa after electromagnetic-induced fission are shown. The charge yields are normalized to 200 %. The lower part displays the corresponding local even-odd effect $\delta(Z)$ as a measure of the local deviation from a Gaussian-like distribution. The line represents a model prediction with a statistical contribution included (see text).**

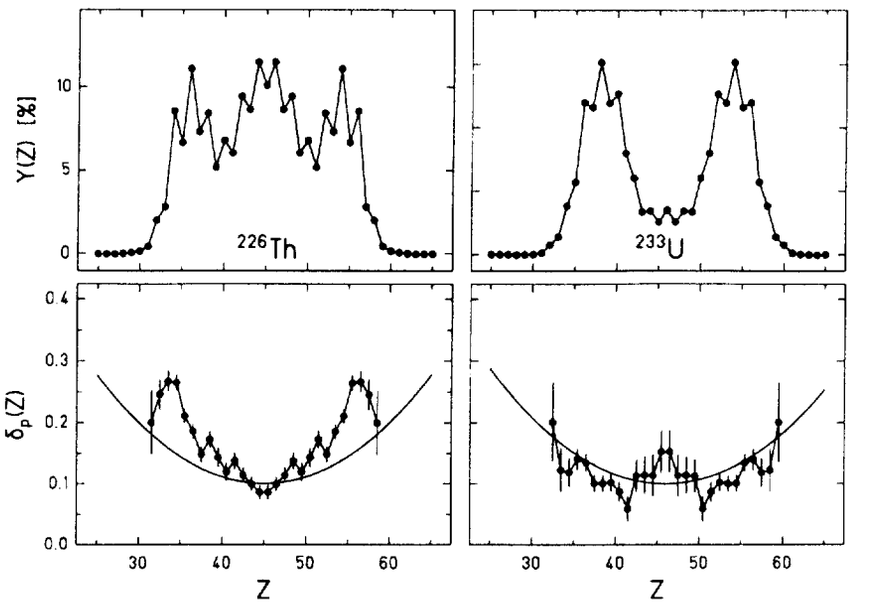

FIGURE 11: **In the upper part, the charge distributions $Y(Z)$ of ^{226}Th and ^{233}U after electromagnetic-induce fission are shown. The charge yields are normalized to 200 %. The lower part displays the corresponding local even-odd effect $\delta(Z)$ as a measure of the local deviation from a Gaussian-like distribution. The line represents a model prediction with a statistical contribution included (see text).**

the even-odd effect with decreasing fissility parameter Z_{CN}^2/A_{CN} observed between ^{252}Cf and ^{232}Th can partly be attributed to an increasing statistical contribution, because the asymmetry parameter $(Z_{heavy} - Z_{light})/Z_{CN}$ on the average increases from ^{252}Cf. to ^{232}Th, due to the stationary position of the heavy component in the mass distributions near A = 138.

The new findings reveal that the enhanced production of fission fragments with even proton numbers cannot directly be interpreted as the probability that no quasiparticle excitations up to the scission point are induced. The relation between the even-odd effect and the intrinsic excitation energy at scission is more complex than assumed previously.

CONCLUSION

The present work reports on the first application of secondary beams for nuclear-fission studies. The experiments had to combine several stages in a rather complex way. First, the nuclei of interest had to be produced, separated and identified. Their production cross sections were determined. Secondly, excited states in the vicinity of the fission barrier were populated by electromagnetic interactions in a lead target. Finally, the fission fragments were registered, and their elemental yields as well as their total kinetic energies were determined. In view of the low primary-beam intensity of less than 10^7 projectiles per second, the success of the experiment essentially depended on the application of a very efficient excitation mechanism and on a high detection probability of the experimental set up. In contrast to most secondary-beam experiments of the first generation which are designed to determine a specific property of the secondary projectiles like binding energy or total interaction cross section, the present experiment is a true secondary-reaction study where many characteristics of the fission process could be investigated.

The main advantages of the secondary-beam experiment are the rather free choice of the nucleus to be investigated, independent of its chemical properties and independent of its radioactive decay characteristics, the excellent nuclear-charge resolution achieved for all fission fragments, and the remarkably good determination of the total kinetic energies where structural effects in the order of 10^{-5} of the laboratory energies could be observed. In particular, the large number of high-quality nuclear-charge distributions reveales the important progress attained by the new experimental technique.

The influence of fission competition on the fragmentation cross sections revealed new information on the level densitiy in spherical, transitional, and deformed nuclei. Evidence for the loss of collectivity of nuclear excitations at energies around 40 MeV has been found. The damping of the collective enhancement in the nuclear level density was found to be independent of nuclear deformation. It was shown that the influence of shell stabilization and collective enhancement on the fission competition of spherical nuclei near N = 126 cancel each other. Therefore, estimations of the production cross sections of spherical superheavy nuclei near the 184-neutron shell which are based on the intrinsic level density without inclusion of the collective enhancement are expected to be by far too optimistic.

The first secondary-beam experiments on nuclear fission provided the elemental yields and the total kinetic energies for the low-energy fission of a large number of short-lived radioactive nuclei. The beautiful data nicely demonstrate the decisive influence of nuclear structure on the fission process in a particularly interesting transitional region. The transition from symmetric to asymmetric fission around mass number 227 was explained by

the characteristics of the mass-asymmetry potential at the fission barrier. It seems to be caused by the competition between strong neutron shells corresponding to fragments with 82 and 86 neutrons which favour the asymmetric fission channels (standard I and standard II) and the liquid-drop potential which favours symmetric fission. While the relative strengths of these fission channels vary drastically as a function of mass number of the fissioning system, leading to very different charge distributions, the scission configurations corresponding to these fission channels which are decisive for the total kinetic energies seem to be rather universal.

The new understanding of the even-odd effect in fission deduced from the present data will allow to extract more reliable information on the viscosity of cold nuclear matter. It seems that strong variations of the observed even-odd effect in the elemental yields for different systems and as a function of asymmetry for a specific system are attributed to a great part to a statistical contribution to this quantity rather than to a variation of the intrinsic excitation energy.

REFERENCES

1 T. Enqvist et al., contribution to this conference
2 J. Benlliure, A. Grewe, M. de Jong, K.-H. Schmidt, S. Zhdanov, submitted to Nucl. Phys. **A**
3. S. Bjørnholm, A. Bohr, B. R. Mottelson, Proc. Int. Conf. on the Physics and Chemistry of Fission, Rochester 1973, (IAEA Vienna 1974) Vol. 1, pp. 367
4. G. Hansen and A. S. Jensen, Nucl. Phys. **A406** (1983) 236
5. M de Jong, A. V. Ignatyuk, K.-H. Schmidt, Nucl. Phys. **A613** (1997) 435
6 V. V. Pashkevich, Nucl. Phys. **A169** (1971) 275
7. C. Brosa, S. Grossmann, A. Müller, Phys. Rep. **197** (1990) 167
8 P. Fong, Phys. Rev. **102** (1956) 434
9. B. D. Wilkins, E. P. Steinberg, R. R. Chasman, Phys. Rev. **C14** (1976) 1832
10. P. Möller, S. G. Nilsson, Phys. Lett. 31B (1970) 283
11 H. Kudo, H. Muramatsu, H. Nakahara, K. Miyano, I. Kohno, Phys. Rev. C 25 (1982) 3011
12 G. A. Kudyaev, Yu. B. Ostapenko, G. N. Smirenkin, Yad. Fiz. **45** (1987) 1534 (Sov. J. Nucl. Phys. **45** (1987) 951)
13. G. A. Kudyaev, Yu. B. Ostapenko, E. M. Rastopchin, Yad. Fiz. **47** (1988) 1540 (Sov. J. Nucl. Phys. **47** (1988) 976)
14. E. K. Hulet, J. F. Wild, R. J. Dougan, R. W. Lougheed, J. H. Landrum, A. D. Dougan, P. A. Baisden, C. M. Henderson, R. J. Dupzyk, R. L. Hahn, M. Schädel, K. Sümmerer, G. Behune, Phys. Rev. Lett. **56** (1986) 313
15. E. K. Hulet, J. F. Wild, R. J. Dougan, R. W. Lougheed, J. H. Landrum, A. D. Dougan, P. A. Baisden, C. M. Henderson, R. J. Dupzyk, R. L. Hahn, M. Schädel, K. Sümmerer, G. Bethune, Phys. Rev. **C40** (1989) 770
16. D. C. Hofmann, Nucl. Phys. **A502** (1989) 21c
17. P. Möller, J. R. Nix, Proc. Symp. on Phys. and Chem. of Fission, Rochester 1973, vol 1, (Vienna, IAEA, 1974) pp 329
18. M. G. Mustafa, U. Mosel, H. W. Schmitt, Phys. Rev. **C7** (1973) 1519
19. V. V. Pashkevich, Nucl. Phys. **A477** (1988) 1
20. S. Cwiok, P. Rozmej, A. Sobiczewski, Z. Patyk, Nucl. Phys. **A491** (1989) 281
21. R. C. Jensen, A. W. Fairhall, Phys. Rev. **109** (1958) 942
22. H. C. Britt, H. E. Wegner, J. C. Gursky, Phys. Rev. **129** (1963) 2239
23. J. P. Unik, J. R. Huizenga, Phys. Rev. **B134** (1964) 90
24. E. Konecny, H. W. Schmitt, Phys. Rev. **172** (1968) 1213
25. E. Konecny, H.-J. Specht, J. Weber, Phys. Lett. **B45** (1973) 329
26. H. J. Specht, Rev. Mod. Phys. **46** (1974) 773
27 H. J. Specht, Phys. Scripta **A10** (1974) 21
28. J. Weber, H. C. Britt, A. Gavron, E. Konecny, J. B. Wilhelmy, Phys. Rev. **C13** (1976) 2413

29. M. G. Itkis, Yu. Ts. Oganessian, G. Chubarian, V. N. Okolovich, G. N. Smirenkin, in Nuclear Fission and Fission-product Spectroscopy, H. Faust and G. Fioni (eds.), ILL Grenoble (1994) pp. 77
30. M. Itkis, V. N. Okolovich, A. Ya. Rusanov, G. N. Smirenkin, Sov. J. Nucl. Phys. **41** (1985) 544
31. H. Nifenecker, G. Mariolopoulos, J. P. Bocquet, Z. Phys. **A308** (1982) 39
32. H. Geissel, P. Armbruster, K.-H. Behr, A. Brünle, K. Burkard, M. Chen, H. Folger, B. Franczak, H. Keller, O.Klepper, B. Langenbeck, F. Nickel, F. Pfeng, M. Pfützner, E. Roeckl, K. Rykaczewski, I. Schall, D. Schardt, C. Scheidenberger, K.-H. Schmidt, A. Schröter, T. Schwab, K. Sümmerer, M. Weber, G. Münzenberg, T. Brohm, H.-G. Clerc, M. Fauerbach, J.-J. Gaimard, A. Grewe, E. Hanelt, B. Knödler, M. Steiner, B. Voss, J. Weckenmann, C. Ziegler, A. Magel, H. Wollnik, J.P. Dufour, Y. Fujita, D. J. Vieira, B. Sherrill, Nucl, Instr. Meth. **B70** (1992) 286
33. H.-G. Clerc, M. deJong, T. Brohm, M. Dornik, A. Grewe, E. Hanelt, A. Heinz, A. R. Junghans, C. Röhl, S. Steinhäuser, B. Voss, C. Ziegler, K.-H. Schmidt, S. Cyajkowski, H. Geissel, H. Irnich, A. Magel, G. Münzenberg, F. Nickel, A. Piechacyek, C. Scheidenberger, W. Schwab, K. Sümmerer, W. Trinder, M. Pfützner, B. Blank, A. Ignatyuk, G. Kudyaev, Nucl. Phys. **A590** (1995) 785
34. A. R. Junghans, M. de Jong, H.-G. Clerc, A. V. Ignatyuk, G. A.Kudyaev, K.-H. Schmidt, accepted for publication by Nucl. Phys. A
35. K.-H. Schmidt, E. Hanelt, H. Geissel, G. Münzenberg, J.-P. Dufour, Nucl. Instr. Meth. **A260** (1987) 287
36. B. Voss, T. Brohm, H.-G. Clerc, A. Grewe, E. Hanelt, A. Heinz, M. deJong, A. R. Junghans, W. Morawek, C. Röhl, S. Steinhäuser, C. Ziegler, K.-H. Schmidt, K.-H. Behr, H. Geissel, G. Münzenberg, F. Nickel, C. Scheidenberger, K. Sümmerer, A. Magel, M. Pfützner, Nucl. Instr. Meth **A364** (1995) 150
37. M. de Jong, K.-H. Schmidt, B. Blank, C. Böckstiegel, T. Brohm, H.-G. Clerc, S. Czajkowski, M. Dornik, H. Geissel, A. Grewe, E. Hanelt, A. Heinz, H. Irnich, A. R. Junghans, A. Magel, G. Münzenberg, F. Nickel, M. Pfützner, A. Piechaczek, C. Scheidenberger, W. Schwab, S. Steinhäuser, K. Sümmerer, W. Trinder, B. Voss, C. Ziegler, Nucl. Phys. **A628** (1998) 479
38. A. Grewe, S. Andriamonje, C. Böckstiegel, T. Brohm, H.-G. Clerc, S. Czajkowski, E. Hanelt, A. Heinz, M. G. Itkis, M. de Jong, M. S. Pravikoff, K.-H. Schmidt, W. Schwab, S. Steinhäuser, K. Sümmerer, B. Voss, Nucl. Phys. **A614** (1997) 400
39. C. Böckstiegel, S. Steinhäuser, J. Benlliure, H.-G. Clerc, A. Grewe, A. Heinz, M. de Jong, A. R. Junghans, J. Müller, K.-H. Schmidt , Phys. Lett **B398** (1997) 259
40. J.-J. Gaimard, K.-H. Schmidt, Nucl. Phys. **A531** (1991) 709
41. A. V. Ignatyuk, G. A. Kudyaev, A. Junghans, M. de Jong, H.-G. Clerc, K.-H. Schmidt, Nucl. Phys. **A593** (1995) 519
42. M. G. Itkis, V. N. Okolovich, A.Ya. Rusanov, G. N. Smirenkin, Sov. J. Part. Nucl. **19** (1988) 301
43. J. Benlliure, A. Grewe, M. de Jong, K.-H. Schmidt, S. Zhdanov, accepted for publication by Nucl. Phys. A
44. B. L. Tracy, J. Chaumont, R. Klapisch, J. M. Nitschke, A. M. Poskanzer, E. Roeckl, C. Thibault, Phys. Rev. **C5** (1972) 222
45. J. L. Sida, P. Armbruster, M. Bernas, J. P. Bocquet, R. Brissot, H. R. Faust, Nucl. Phys. **A502** (1989) 233c
46. R. Hentzschel, H. R. Faust, H. O. Denschlag, B. D. Wilkins, J. Gindler, Nucl. Phys. **A571** (1994) 427
47. V. M. Strutinsky, Contr. to Intern. Conf. on Nucl. Phys. (Paris 1958), pp. 617
48. S. Steinhäuser, J. Benlliure, C. Böckstiegel, H.-G. Clerc, A. Heinz, A. Grewe, M. deJong, A. R. Junghans, J. Müller, M. Pfützner, K.-H. Schmidt, accepted for publication by Nucl. Phys. A